Journal of
Ceramic Science
and Technology

J. Ceram. Sci. Technol., **11** [1] 27-35 (2020)
DOI: 10.4416/JCST2019-00053
available online at: http://www.ceramic-science.com

Fabrication and Dielectric Properties of $LiTaO_3$ Matrix Ceramics with Added Manganese Dioxide

Y. Yao, Y. Zhang*

School of Materials Engineering, Shanghai University of Engineering Science, P. R. China
received August 15, 2019; received in revised form November 2, 2019; accepted November 8, 2019

Abstract

Polycrystalline $LiTaO_3$ ceramics are beset with difficulties with regard to fabrication by means of conventional pressureless sintering because of their own refractory character. In this study, composite ceramics of $LiTaO_3$ with added manganese dioxide were obtained by sintering at 1 250 °C. The sinterability, microstructure and dielectric properties of the $LiTaO_3$ composite ceramics were then investigated. The relative densities of the $LiTaO_3$ composite ceramics were significantly improved by the addition of MnO_2 powder. The $LiTaO_3$ composite ceramics achieved the highest relative density (93.1 %) and obtained a well-grained microstructure when the amount of MnO_2 added was 5 wt%. Only the $LiTaO_3$ phase in the composite ceramics was observed when the MnO_2 content added was less than 3 wt%. The second phase of the Mn_3O_4 particles existed in the boundaries of the $LiTaO_3$ grains, and the content gradually increased when the mass fraction of added MnO_2 was more than 3 wt%. The effects of the MnO_2 added on the dielectric properties of the $LiTaO_3$ composite ceramics are studied thoroughly herein. Consequently, the dielectric constant was found to be enhanced, and the dielectric loss decreased in the $LiTaO_3$ composite ceramics with the MnO_2 addition (i.e. both frequency- and temperature-dependent). The optimum values of the relative density, microstructure and dielectric properties were obtained when 5 wt% MnO_2 was added to the $LiTaO_3$ composite ceramics.

Keywords: $LiTaO_3$ ceramics, manganese dioxide, microstructure, dielectric properties

I. Introduction

As an excellent single crystal, lithium tantalite ($LiTaO_3$) has high values of planar electromechanical coupling, mechanical quality factor and low acoustic transmission loss and is used in various applications because of its low dielectric constant [1–3]. Many studies have focused on the single crystals of $LiTaO_3$ [4–8], whilst only a few have discussed the fabrication, sintering and dielectric properties of $LiTaO_3$ ceramics [9–12] because $LiTaO_3$ is beset with difficulties as regards densification in the sintering process. Previous studies have tried to facilitate sintering of $LiTaO_3$ ceramics with the addition of oxides/fluorides or doping in two steps comprising powder synthesis, followed by sintering [13–14]. Many studies on $LiTaO_3$ solid solution systems, such as the $CaTiO_3$-doped $LiTaO_3$ system, the LiF and MgF_2 co-doped $LiTaO_3$ system, the Mg-doped $LiTaO_3$ system and $Li_{(1-x)}Ag_xTaO_3$, have also been performed [13,15–17]. S. Shimada *et al.* found that MnO_2 is an efficient sintering aid in comparison with other oxides, but its microstructure and other properties were not systematically investigated [14]. Mn is a good element that can improve the performance of many functional ceramics. Accordingly, researchers have shown that doping with Mn can improve the dielectric properties of ceramics [18–20]. Therefore, MnO_2 was added to fabricate MnO_2/$LiTaO_3$ composite ceramics based on a solid-state sinteringprocess using MnO_2 and $LiTaO_3$ raw powders. $LiTaO_3$ matrix ceramics were successfully fabricated with the addition of different MnO_2 contents. The microstructure and the dielectric properties of the MnO_2/$LiTaO_3$ composite ceramics were investigated.

II. Experimental

$LiTaO_3$ matrix composite ceramics with different MnO_2 contents (mass fractions of 1 %, 3 %, 5 % and 7 %, sample MLT) were manufactured with a conventional sintering method. Commercially available $LiTaO_3$ powder (Fangxiang Industry Co. Ltd., Shanghai, China) and MnO_2 powder (Shanghai Meixing Chemical Co. Ltd., Shanghai, China) were used as the raw materials. On the basis of mass ratio, the two powders were weighed, then ball-milled in alcohol with carnelian balls for 24 h. The blended powders were dried and calcined at 800 °C for 3 h, then mixed with 7.0 wt.% polyvinyl alcohol binder. The powders were ground again after calcination, then pressed into discs with 16 mm diameter and approximately 2 mm thickness. Finally, all the discs were sintered at 1 250 °C for 3 h.

The relative density of the samples was measured with the Archimedes method. The crystalline structure of the samples was obtained by means of an X-ray diffractometer (X'Pert PRO, PANalytical, Holland) using CuK*a* ra-

* Corresponding author: zhangyoufeng@sues.edu.cn

diation. The surface element compositions and the chemical states of the samples were analysed with X-ray photoelectron spectroscopy (XPS, ESCALAB 250Xi, Thermo Fisher) with AlK*a* radiation. Scanning electron microscopy (SEM, Hitachi S-3400N, Japan) with an energy-dispersive spectrometer (EDS) was performed to examine the microstructure and the distribution of the compositions. The samples were plated by means of silver painting on both sides of the polishing pellets, then kept warm at 850 °C for 10 min to characterise their dielectric properties. The frequency-dependent dielectric constant and the dielectric loss were obtained at room temperature from 100 Hz to 1 MHz using an impedance analyser (Model Agilent E4990A, Central South University, Hunan, China). The temperature dependence of the dielectric constant and the dielectric loss were measured with an LCR meter (Model HP4284A, Agilent Technologies Ltd., Hyogo, Japan) at 100 KHz from room temperature to 750 °C.

III. Results and Discussion

Fig. 1 shows the relative density of the $LiTaO_3$ matrix ceramics with different MnO_2 contents. It can be seen from the figure that the relative density increased first and then decreased with the increasing MnO_2 content. The relative density of the composite ceramics first significantly increased with the increasing MnO_2 content when the MnO_2 content was less than 3 wt%, then slowly increased when the MnO_2 content was increased to 5 wt%. It subsequently decreased. The relative density of the pure $LiTaO_3$ ceramic was very low because the anisotropy of the bulk expansion led to the rupture of the grains or boundaries, that is the $LiTaO_3$ itself can hardly undergo densification [9]. The highest value of the relative density of the composite ceramics reached 93.1 %. The addition of MnO_2 can significantly promote the sintering densification process of the $LiTaO_3$ matrix ceramics; however, the addition of excess MnO_2 pulled down the relative density, which could be related to the uniformity of the grain growth during the sintering process. Li *et al.* also reported similar results when studying the effect of MnO_2 on BNBT ceramics [21].

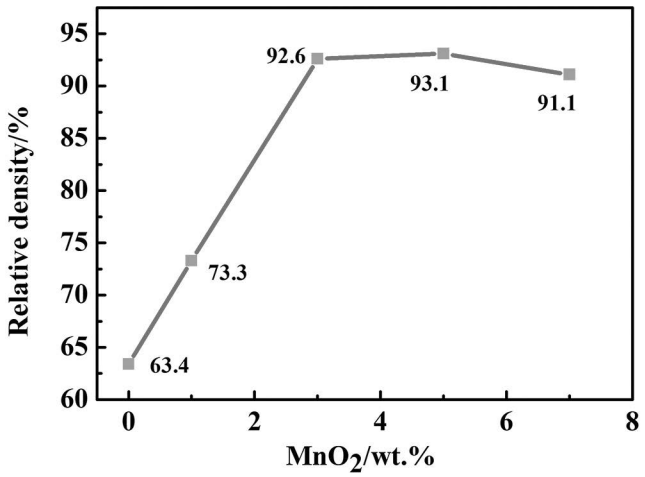

Fig. 1: Relative density of the $LiTaO_3$ composite ceramics.

Fig. 2 shows the XRD patterns of the $LiTaO_3$ matrix ceramics with different MnO_2 contents. Fig. 2(a) illustrates that the $LiTaO_3$ ceramic samples with 1 wt% and 3 wt% MnO_2 contents had a trigonal (rhombohedral) crystal structure. Moreover, no secondary phase occurred, indicating that MnO_2 had probably diffused into the $LiTaO_3$ lattice to form solid solutions, and the addition of MnO_2 did not significantly change the crystal structure of $LiTaO_3$. The XRD results also showed that the $LiTaO_3$ ceramic samples with the added MnO_2 contents of 5 wt% and 7 wt% had a detectable secondary phase, that is Mn_3O_4. In other words, a higher MnO_2 content cannot diffuse into the $LiTaO_3$ lattice and exist as a secondary phase. The fact that Mn ions have different valence states at different temperatures has been demonstrated with the following equation [22]:

$$\overset{+4}{MnO_2} \xrightarrow{535\,^\circ C} \overset{+3}{Mn_2O_3} \xrightarrow{1080\,^\circ C} \overset{+2,+3}{Mn_3O_4} \xrightarrow{1650\,^\circ C} \overset{+2}{MnO} \qquad (1)$$

Mn_3O_4 is present in the $LiTaO_3$ composite ceramics with added MnO_2 contents of 5 wt% and 7 wt% because the sintering temperature was 1 250 °C. Fig. 2(b) shows an enlarged pattern of the (240) diffraction peak of the $LiTaO_3$ crystal. Accordingly, the (240) diffraction peak shifted towards a low angle as the MnO_2 content increased.

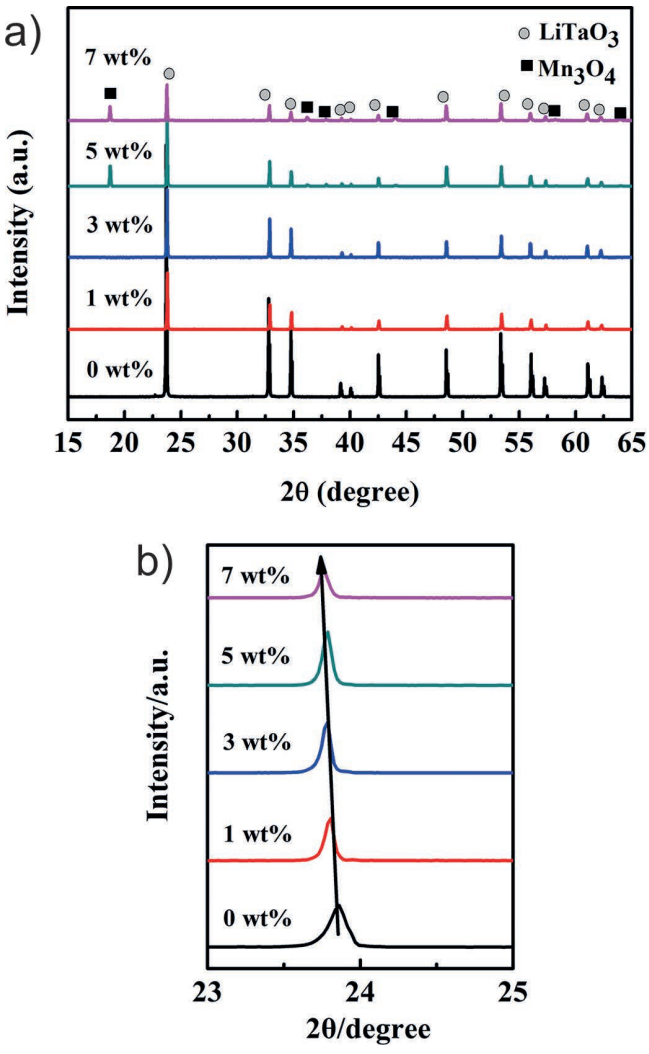

Fig. 2: X-ray diffraction (XRD) patterns of the $LiTaO_3$ ceramics with different MnO_2 contents.

This result indicates that the Mn ions diffused into the $LiTaO_3$ lattices. According to the ionic radius of Mn^{3+}

(0.645 Å), the ionic radius of Mn^{2+} (0.83 Å) and the ionic radius of Ta^{5+} (0.64 Å), it is reasonable that the lattice expansion of the $LiTaO_3$ ceramics should be caused by the replacement of the smaller Ta^{5+} by Mn^{2+} or Mn^{3+}. The similar cation occupancy behaviour has also been reported in other Mn-doped, Pb-based perovskite ceramics [23, 24].

An XPS analysis was performed on the $LiTaO_3$ ceramic with an added 5 wt% MnO_2 to further confirm the composition, electronic configuration and surface state of the samples. The XPS spectra showed that the sample contained the Li, Ta, Mn, O and C elements in the $LiTaO_3$ composite ceramic with 5 wt% MnO_2 content. Calibration of all binding energies was done by referencing the C1s peak BE = 285.0 eV. The spectral lines of the elements agreed well with the elements of the $LiTaO_3$ composite ceramic with the added MnO_2. In other words, no extra element interacted in the specimens.

A further analysis of the region where each element is located is given in Fig. 3(b), which displays the Mn 2p spectra of the $LiTaO_3$ composite ceramic with the added 5 wt% MnO_2. The binding energy of Mn indicated the presence of the Mn 2p1/2 and Mn 2p2/3 electron configurations at 653.6 eV and 641.3 eV, respectively. The main peak of 2p3/2 was located at 641.3 eV. Three $2p_{3/2}$ peaks of the binding energies in the $LiTaO_3$ composite ceramic with an added 5 wt% MnO_2 located at 641.2 eV, 643.2 eV and 646.1 eV and their respective calculated proportions were 66 %, 30 % and 4 %, respectively. The binding energy located at the lower binding energy was attributed to the Mn^{2+} ions, whilst the binding energies located at the higher binding energy were attributed to the Mn^{3+} and Mn^{4+} ions, and similar results were obtained by Cen *et al.* [25]. Therefore, we have reason to believe that Mn ions coexist in MLT ceramics in three valence states. Researchers have reported that Mn ions have different valence states at different temperatures [22]. The existence of Mn^{4+} may be due to the fact that MnO_2 is not fully involved in the reaction. In the O_1s spectrum (Fig. 3c), the binding energy of 530.4 eV belonged to the lattice oxygen (O^{2-}). The peak at 531.8 eV indicates the defects, chemisorbed oxygen and coordinated lattice oxygen [26]. The results show that rich valence and defects exist in $LiTaO_3$ composite ceramics, which is beneficial to the grain growth of the $LiTaO_3$ composite ceramics. The radius of Mn^{3+} is close to that of Ta^{5+} but smaller than that of Ta^{5+}. The substitution of Ta^{5+} at the B site in $LiTaO_3$ increases the lattice constant.

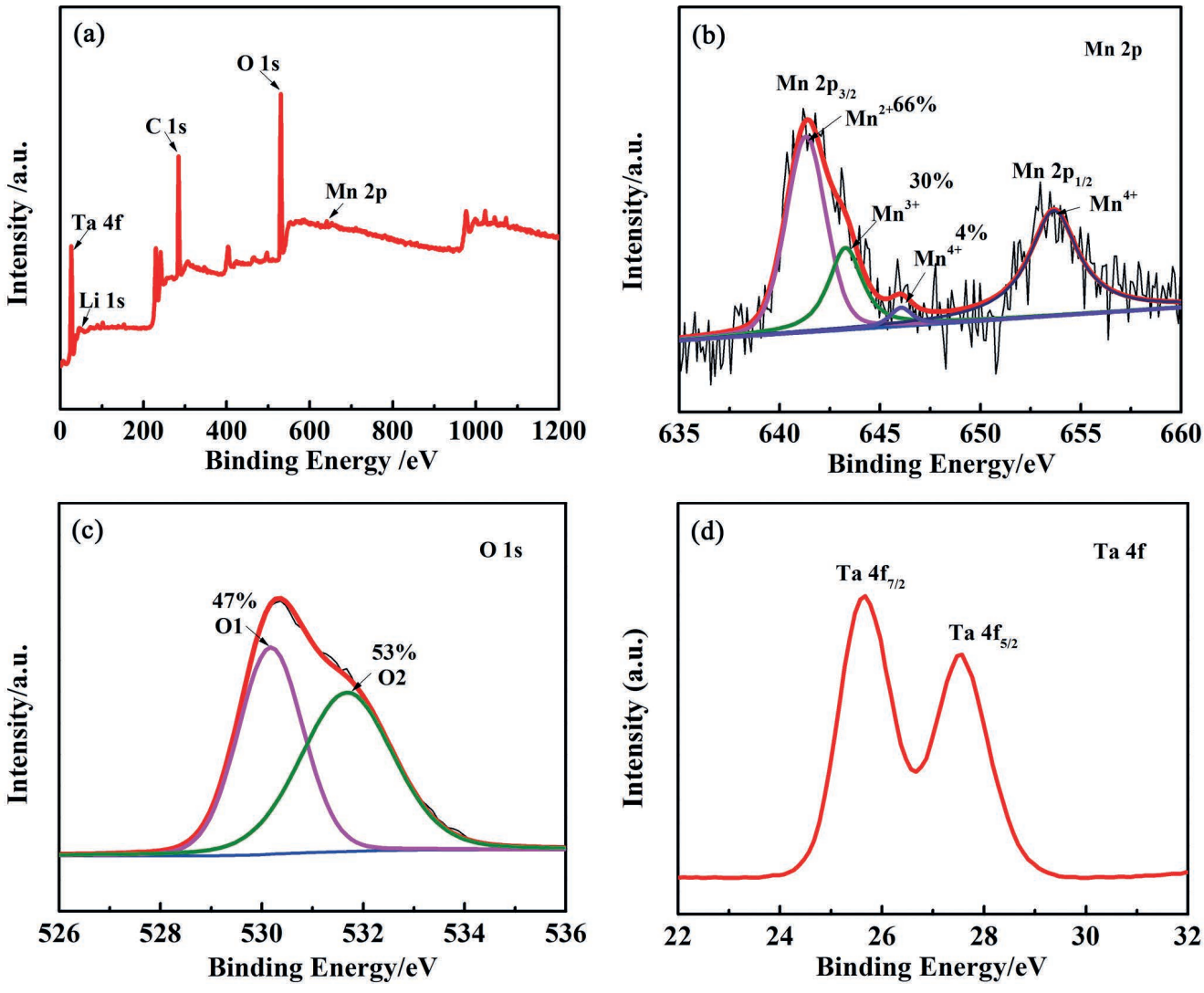

Fig. 3: XPS spectra of 5MLT ceramic a) full spectrum, b) Mn 2p, c) O1s, and d) Ta 4 f.

The O^{2-} radius is much larger than other ions in MLT composite ceramics. MLT composite ceramic sintering is mainly restricted by oxygen ion diffusion. The replacement of Ta^{5+} ions in the $LiTaO_3$ crystal by the Mn cation will generate oxygen vacancies (Vo″), and the oxygen vacancies will promote the migration of ions during sintering and elongate the grain length. The solid solubility of the additive is low, and it not only enters the crystal lattice but also accumulates at the grain boundary. The pores are discharged outward along the grain boundary, so the addition of Mn cation not only promotes the sintering process but also prevents the abnormal growth of crystal grains. The fineness of the crystal grains is uniform, which promotes the increase in density. Wang *et al.* [27] found that in KNN ceramics with the addition of more than 0.5 % Mn defective compounds ($Mn''_{Nb} - Vo''$) and ($Mn'_{Nb} - Vo'' - Mn'_{Nb}$) were formed, the proper amount of defects will promote the uniform growth of crystal grains.

Fig. 4 shows the SEM micrographs of the $LiTaO_3$ composite ceramics with different MnO_2 contents.

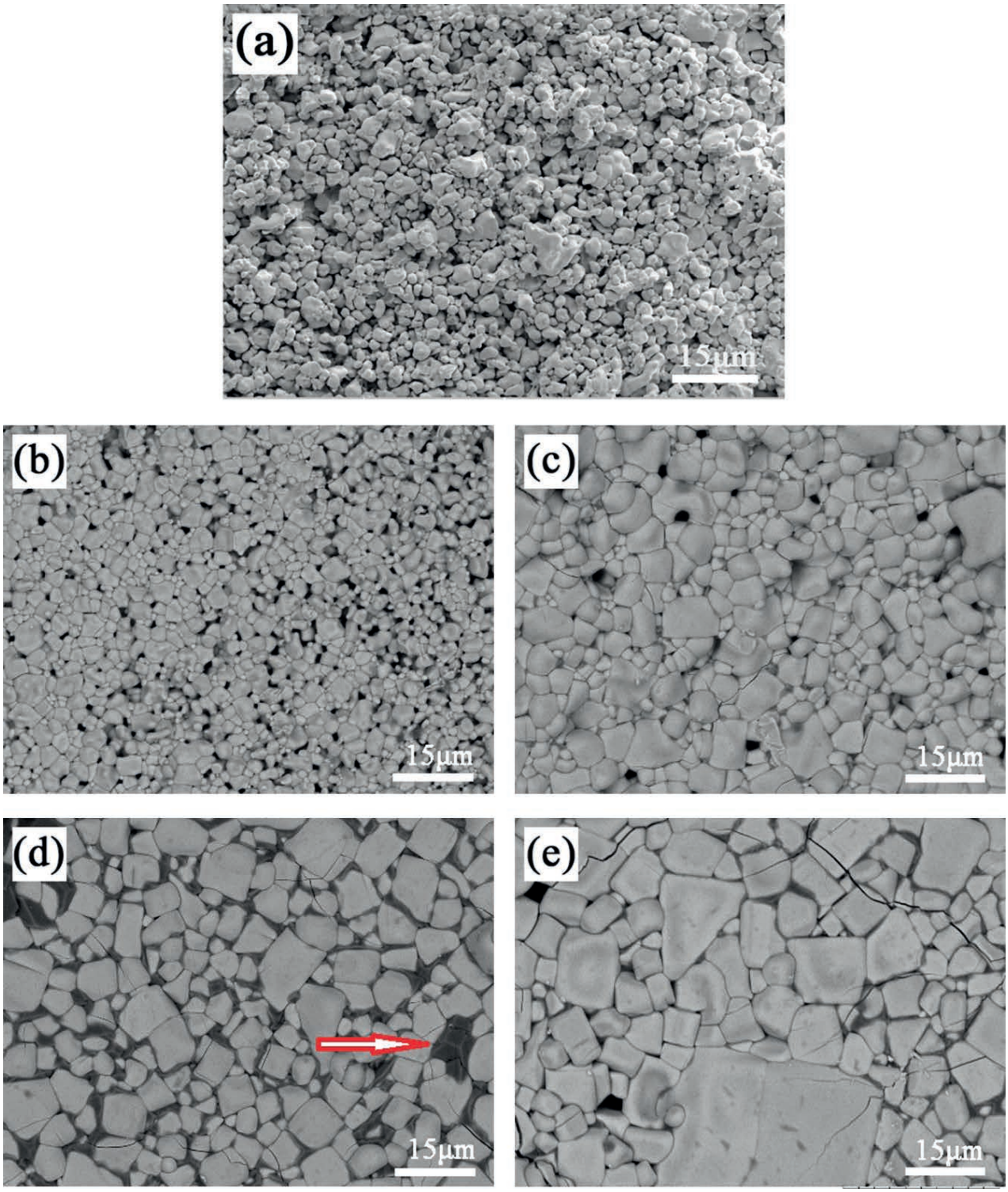

Fig. 4: SEM micrographs of the $LiTaO_3$ composite ceramics with different MnO_2 contents a) 0 wt% b) 1 wt% c) 3 wt% d) 5 wt% d) 7 wt%.

Fig. 4 shows that the porosity of the $LiTaO_3$ composite ceramics with different MnO_2 contents first decreased, then increased with the increasing MnO_2 content. The pores were least when the added MnO_2 amounted to 5 wt%. This result was the same as the trend of relative density. Adding MnO_2 to $LiTaO_3$ could also effectively affect the grain growth. The average particle size of the samples increased with the increased MnO_2 content. Excess manganese oxide existed at the grain boundaries of $LiTaO_3$ when the MnO_2 content was 5 and 7 wt%. In the figure, manganese oxide is represented by an arrow. Abnormal grain growth in the $LiTaO_3$ ceramic can be observed with 7 wt% MnO_2. The grain size of $LiTaO_3$ was uniform, and the second phase homogeneously distributed in the composite 5MLT ceramic because adding Mn cations into the $LiTaO_3$ ceramic leads to a replacement of Ta^{5+} by Mn^{2+}/Mn^{3+}. Accordingly, oxygen vacancies occurred, resulting in easier grain boundary mobility, which is conducive to better sintering behaviour. The addition of an appropriate content of MnO_2 is beneficial to the uniform growth of grains and improves the sintering performance of the $LiTaO_3$ matrix ceramics. However, an excessive amount of MnO_2 leads to abnormal growth of grains and impairs the sintering performance of $LiTaO_3$ matrix ceramics. With increasing MnO_2 content($\leq$ 3 wt%), Mn_3O_4 was not detected in XRD. According to the SEM image, Mn_3O_4 did not appear in 1MLT ceramics, but a small amount of Mn_3O_4 could be seen in the 3MLT ceramics, owing to the small concentration, Mn_3O_4 was not detected in XRD. Fig. 4 shows that MnO_2 diffused into the $LiTaO_3$ lattice to form solid solutions, and the addition of MnO_2 did not give rise to obvious change in the crystal structure and micrograph of the $LiTaO_3$ composite ceramics. The secondary phase was observed in Figs. 4(d) and (e) with a further increase in the added MnO_2. The grey particles denote the $LiTaO_3$ phase, whilst the black prismatic particles represent the manganese oxide that appeared at the grain boundaries. These findings were found to be in accordance with the above-mentioned XRD results. The EDS result is shown in Fig. 5 to determine the composition of the secondary-phase particles. The secondary phase (i.e. black prismatic particles) was a Mn_3O_4 phase according to the combined XRD and EDS results.

Fig. 6 shows the EDS mapping of 3MLT composite ceramics. Li element cannot be detected in EDS, because Li element is a lightweight element [28]. It can be seen from the figure that there are more pores on the ceramic surface, and the distribution of O element is relatively uniform. According to the results of EDS mapping, it is found that Mn element is relatively uniform. An analysis based on a combination with the XRD results suggests that Mn ions have been diffused into $LiTaO_3$ crystal.

The variation of dielectric constant and dielectric loss with the frequency range from 100 Hz to 1 MHz at room temperature is shown in Fig. 7. It can be seen from Fig. 7(a) that the dielectric constant gradually decreases with the increase of frequency in the frequency range of 100 Hz – 10 kHz. The dielectric constant almost approaches a stable value in the frequency range of 10 kHz – 1 MHz. The dielectric constant first increased,

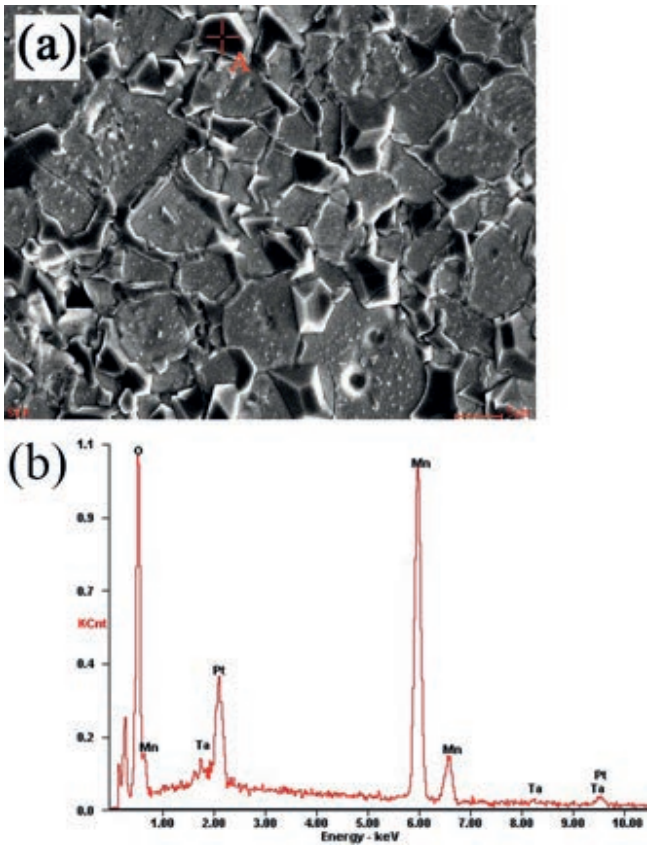

Fig. 5: SEM micrograph a) and EDS result b) of point A in 5MLT.

then decreased with the increasing MnO_2 content at the same frequency. Subsequently, it achieved the maximum value of 44 when the MnO_2 content was 5 wt%. Fig. 7(b) shows that the dielectric loss of all investigated samples decreased with the increase of the test frequency, and the dielectric loss first decreased, then increased with the increasing MnO_2 content at the same frequency. It then achieved the minimum value when the MnO_2 content was 5 wt%. The dielectric constant was the largest, whilst the dielectric loss was the smallest when 5 wt% MnO_2 had been added to the $LiTaO_3$ ceramic. The dielectric properties were affected by many factors, for instance porosity, second phase and ionic polarisabilities [29]. The SEM results showed that the pores were gradually eliminated, and a fine microstructure was obtained with the increasing MnO_2 content, which led to the enhanced dielectric constant. The dielectric constant decreased when more than 5 wt% MnO_2 was added because of the grain inhomogeneity and the worsening sinterability. Similarly, the dielectric loss was the lowest when 5 wt% MnO_2 was added. The low dielectric loss may be caused by an increase in density because there are fewer pores in the ceramic with high density, resulting in less space charge accumulated in the pores, and the lower spatial polarization of the ceramic. When the addition amount of MnO_2 is 7 wt%, the density is low, and the sintering property deteriorates compared with the addition amount of 5 wt%. The pores are also relatively large, and the crystal grain size grows abnormally. The number of defects increases as the number of holes increases, resulting in a decrease in dielectric constant and a large dielectric loss.

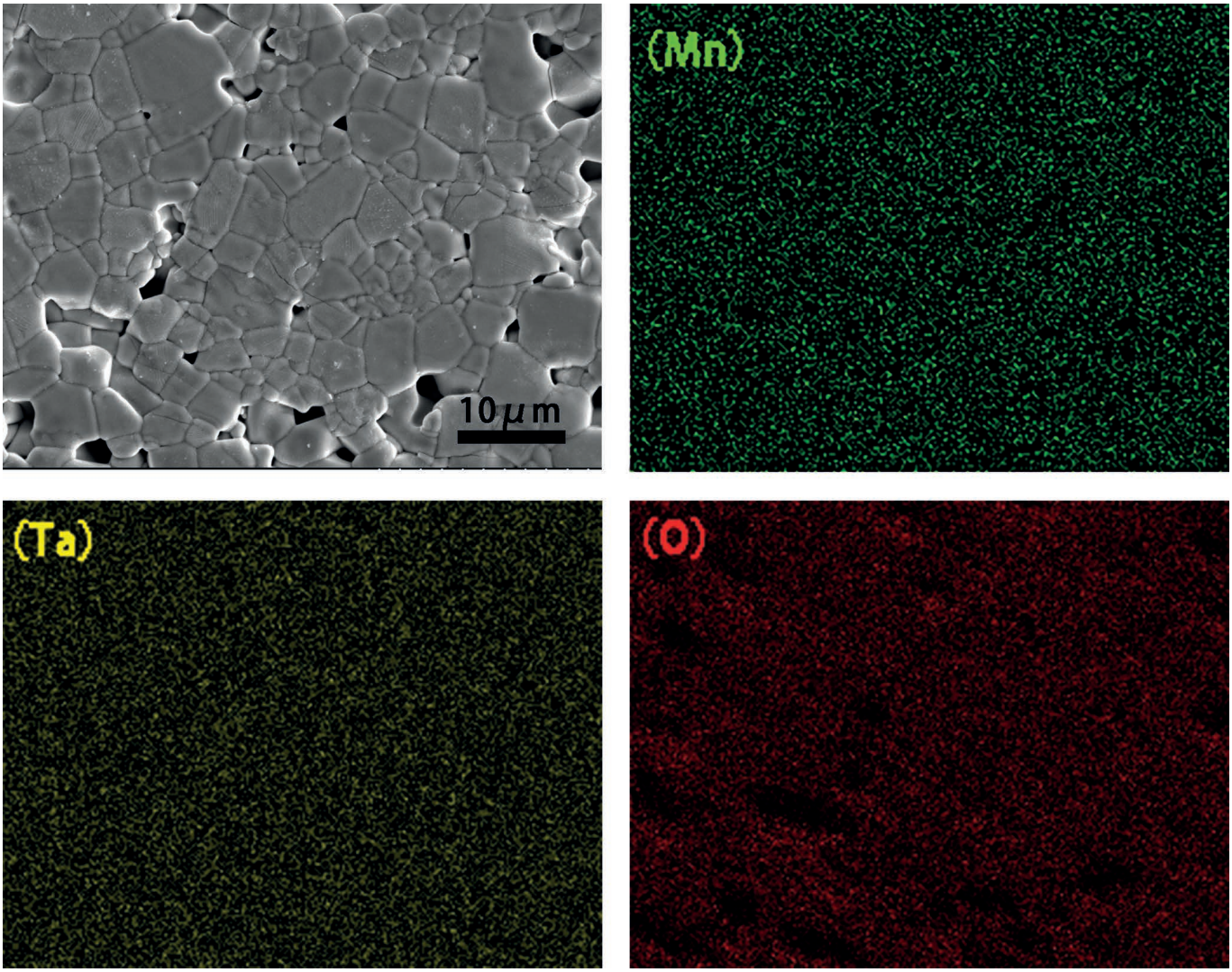

Fig. 6: EDS mapping of 3MLT composite ceramics.

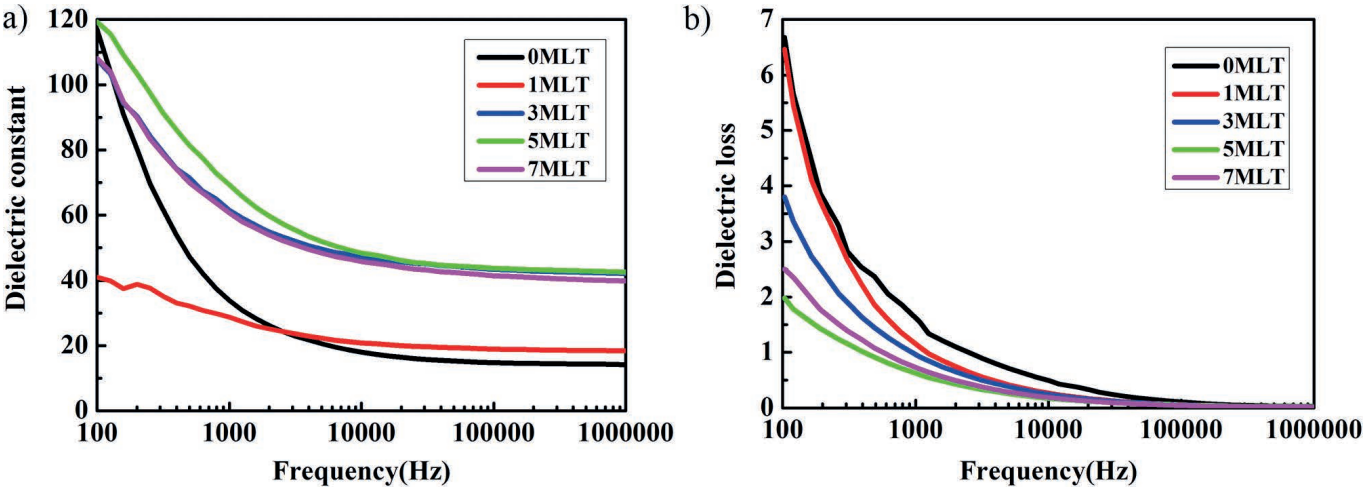

Fig. 7: The frequency-dependent dielectric constant a) and dielectric loss b) of the $LiTaO_3$ composite ceramics.

The temperature-dependent dielectric constant (ε_r) and the dielectric loss (tanδ) of the 5MLT ceramics as a function of the temperature were measured at 100 Hz. Figs. 8 and 9 show the result. The maximum dielectric constant gradually increased by up to 3 280 at 5MLT, then decreased. Furthermore, only one peak appeared in the $LiTaO_3$ composite ceramics with different MnO_2 contents. The variation in the dielectric permittivity behaviour can scarcely be related only to the differences in the microstructure. The observed variation in permittivity could be related to the porosity and non-uniform microstructure of the whole samples. The dielectric constant first increased in the samples, then decreased with the increase of the addition amount of MnO_2. These results could be ascribed to the densification, grain configuration and observed uniform distribution of the secondary phase throughout the specimens. An obvious difference was noticed in the dielectric behaviour between samples with less and more added MnO_2. A pronounced permittivity-temperature response and a rapid phase transition from the ferroelectric to the paraelectric phase at the Curie temperature (*Tc*), wherein $LiTaO_3$ was transformed from a trigonal to a tetragonal system, were observed for the samples with a higher MnO_2 content. A small variation in the dielectric permittivity at the Curie temperature and an almost flat and stable permittivity response of the dielectric constant were noticed for the samples with a lower MnO_2. The inset of Fig. 8 shows the variation of the Curie temperature versus different MnO_2 contents.

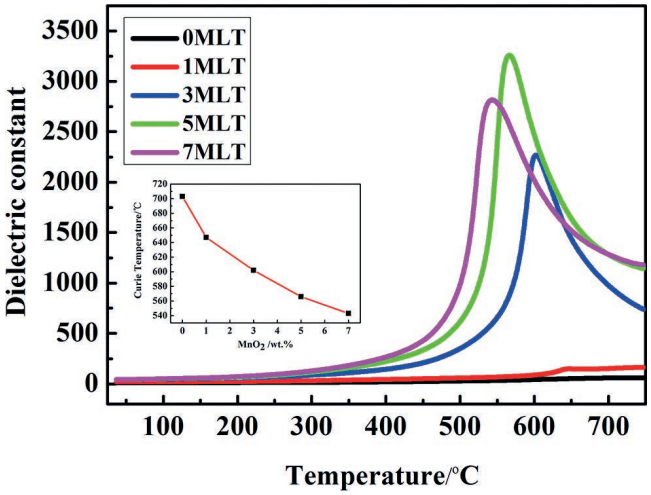

Fig. 8: The temperature dependence of the dielectric constant of the $LiTaO_3$ composite ceramics at 100 kHz.

The permittivity-temperature detection indicated that the Curie temperature was in the range of 703 – 647 °C, which was lower (i.e. it shifted to a lower temperature with the increase in the MnO_2 content from 0 to 7 wt%). The Curie temperatures of the $LiTaO_3$ composite ceramics were 703, 647, 602, 566 and 543 °C. The Curie temperature decreased with the increase in the solid solubility or the replacement of Ta^{5+} by Mn^{2+}/Mn^{3+} at the B site. The replacement at the B site by Mn^{2+}/Mn^{3+} could create oxygen vacancies. The occurrence of oxygen vacancies broke the original symmetrical structure according to research on the dielectric properties of oxygen vacancies in the X8R system by Sun *et al.*, thereby improving the stability of the paraelectric phase (i.e. the Curie temperature point shifted in the low-temperature direction) [30].

Fig. 9 shows that the dielectric loss of the $LiTaO_3$ composite ceramics with different MnO_2 contents increased with increasing temperature. The dielectric loss first decreased, then increased with increasing MnO_2 content. The dielectric loss significantly increased when the temperature was over 400 °C in the $LiTaO_3$ composite ceramics with the MnO_2 content of 0, 1 and 7 wt%, respectively. In other words, the pores and defects resulted in a higher conductivity in the samples with more than three components. The loss of 5MLT was the lowest and the most stable among all the components because of lower porosity and well-grained microstructure. The variation tendency of the dielectric loss versus the component was consistent with the dielectric constant in the temperature range of room temperature to 750 °C.

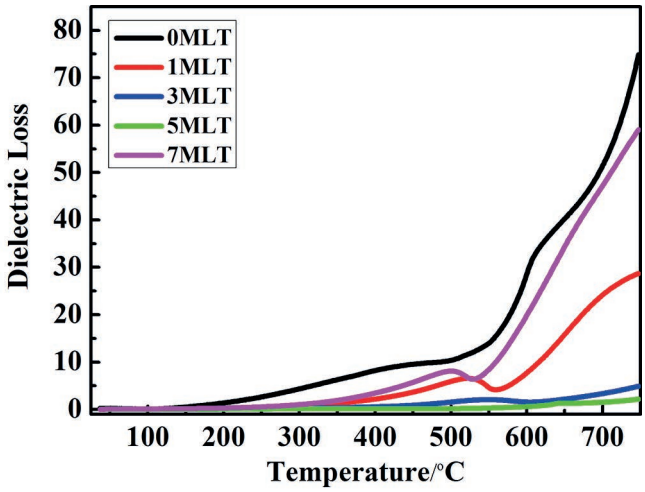

Fig. 9: The temperature dependence of the dielectric loss of the $LiTaO_3$ composite ceramics at 100 kHz.

Fig. 10 presents the ε_r and tanδ of the 5MLT ceramics as a function of temperature at frequencies 0.1, 1, 10, 100 kHz, and 1 MHz. It can be seen from the figure that with the increase in frequency, the dielectric constant of 5MLT ceramic composite gradually flattens with the change of temperature, which means that there is a "dielectric dispersion phenomenon" [31]. It can be seen from the figure that the dielectric constant increases with the increase in the temperature when it is lower than the Curie temperature, and the increased amplitude of low frequency is larger than that of high frequency. The dielectric constant decreases with the increase of temperature when the temperature exceeds the Curie temperature.

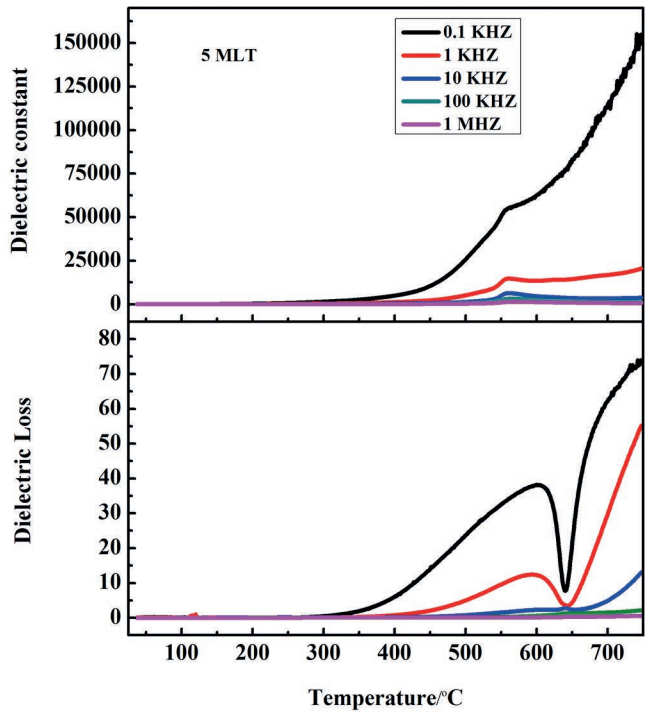

Fig. 10: The temperature dependence of the dielectric constant and loss of the 5MLT composite ceramics at different frequencies.

IV. Conclusions

In summary, $LiTaO_3$ matrix composite ceramics were successfully fabricated by means of pressureless sintering at 1 250 °C. The effects of different MnO_2 contents on the sinterability, microstructure and dielectric properties of the composite ceramics were investigated. The sinterability of the $LiTaO_3$ composite ceramics was improved by increasing the MnO_2 addition. The relative densities of the $LiTaO_3$ composite ceramics were also significantly improved by the addition of MnO_2 powder. The $LiTaO_3$ composite ceramics achieved the highest relative density (93.1 %) and obtained a well-grained microstructure when the amount of added MnO_2 was 5 wt%. The 1MLT and 3MLT ceramics only had the diffraction peaks of $LiTaO_3$, whilst the diffraction peaks of Mn_3O_4 were found in the 5MLT and 7MLT ceramics, indicating that excess MnO_2 was sintered at 1 250 °C in the form of Mn_3O_4, and the content of the Mn_3O_4 particles gradually increased. The grain size of the $LiTaO_3$ composite ceramics continuously increased with the increase in the mass fraction of MnO_2, which can effectively promote grain growth. The dielectric constant of the $LiTaO_3$ composite ceramics at room temperature in the frequency range from 100 Hz to 1 MHz first increased, then decreased with the increase in the MnO_2 content at the same frequency. It also achieved the maximum value of 44 when the MnO_2 content was 5 wt%. Similarly, the dielectric loss was the lowest when the added MnO_2 was 5 wt%. The maximum dielectric constant gradually increased up to 3 280 at 5MLT, then decreased. The Curie temperature decreased with the increase of the additive amount of MnO_2, thereby shifting to a lower temperature with the MnO_2 content increasing from 0 to 7 wt%. The variation tendency of the dielectric loss versus the component was consistent with the dielectric constant in the temperature range of room temperature to 750 °C. Therefore, the highest relative density, well-grained microstructure and better dielectric properties were obtained in 5 wt% MnO_2-added $LiTaO_3$ composite ceramics.

Acknowledgements

This work was supported by the Chinese Nature Science Foundation (No. 11604204 and 51603120).

References

1 Ma, T.F., Wang, J., Du, J., Yuan, L.L., Qian, Z.H., Zhang, Z.T., Zhang, C.: A lateral field excited (yxl)88° $LiTaO_3$ bulk acoustic wave sensor with interdigital electrodes, *Ultrasonics*, **53**, [3], 648 – 651, (2013).

2 Fukuda, T., Matsumura, S., Hirano, H., Ito, T.: Growth of $LiTaO_3$ single crystal for saw device applications, *J. Cryst. Growth.*, **46**, [2], 179 – 184, (1979).

3 Satoh, Y., Kawasaki, D., Yamanouchi, K.: High-coupling and high-temperature stable surface acoustic wave substrates using groove-type interdigital transducer, *Jpn. J. Appl. Phys.*, **45**, [5B], 4658 – 4661, (2006).

4 Gruber, M., Konetschnik, R., Popov, M., Spitaler, J., Supancic, P., Kiener, D., Bermejo, R.: Atomistic origins of the differences in anisotropic fracture behaviour of $LiTaO_3$, and $LiNbO_3$ single crystals, *Acta Mater.*, **150**, 373 – 380, (2018).

5 Gruber, M., Kraleva, I., Supancic, P., Bielen, J., Kiener, D., Bermejo, R.: Strength distribution and fracture analyses of $LiNbO_3$ and $LiTaO_3$ single crystals under biaxial loading, *J. Eur. Ceram. Soc.*, **37**, [14], 4397 – 4406, (2017).

6 Fukuda, T., Matsumura, S., Hirano, H., Ito, T.: Growth of $LiTaO_3$ single crystal for saw device applications, *J. Cryst. Growth.*, **46**, [2], 179 – 184, (1979).

7 Sinclair, D.C., West, A.R.: Electrical properties of a $LiTaO_3$ single crystal, *Phys. Rev. B: Condens. Matter.*, **39**, [18], 13486 – 13492, (1989).

8 Reichenbach, P., Kampfe, T., Thiessen, A., Haussmann, A., Woike, T., Eng, L.M.: Multiphoton photoluminescence contrast in switched Mg:$LiNbO_3$ and Mg:$LiTaO_3$ single crystals, *Appl. Phys. Lett.*,**105**, [12], 122906(1 – 5), (2014).

9 Chen, C.F., Brennecka, G.L., King, G., Tegtmeier, E.L., Holesinger, T., Ivy, J., Yang, P.: Processing of crack-free high density polycrystalline $LiTaO_3$ ceramics, *J. Mater. Sci. Mater. Electron.*, **28**, [4], 3725 – 3732, (2017).

10 Zainuddin, L.W., Kamarulzaman, N.: Effect of sintering time on the purity and morphology of $LiTaO_3$, *Adv. Mater. Res.*, **501**, 129 – 132, (2012).

11 Bomlai, P., Sinsap, P., Muensit, S., Milne, S.J.: Effect of MnO on the phase development, microstructures, and dielectric properties of $0.95Na_{0.5}K_{0.5}NbO_3$–$0.05LiTaO_3$ ceramics, *J. Am. Ceram. Soc.*, **91**, [2], 624 – 627, (2008).

12 Zhou, J.J., Li, J.F., Wang, K., Zhang, X.W.: Phase structure and electrical properties of (Li,Ta)-doped (K,Na)NbO_3 lead-free piezoceramics in the vicinity of Na/K = 50/50, *J. Mater. Sci.*, **46**, [15], 5111 – 5116, (2011).

13 Ye, Z.G., Von Der Mühll, R., Ravez, J.: New oxyfluorides and highly densified ceramics related to $LiNbO_3$, *J. Phys. Chem. Solids.*, **50**, [8], 809 – 812, (1989).

14 Shimada, S., Kodaira, K., Matsushita, T.: Sintering $LiTaO_3$ and $KTaO_3$ with the aid of manganese oxide, *J. Mater. Sci.*, **19**, [4], 1385 – 1390, (1984).

15 Bamba, N., Yokouchi, T., Takaoka, J., Elouadi, B., Fukami, T.: Effects of $CaTiO_3$ on electrical properties in $LiTaO_3$ ceramics, *Ferroelectrics*, **304**, [1], 135 – 138, (2004)

16 Huanosta, A., Alvarez, E., Villafuerte-Castrejón, M.E., West, A.R.: Electrical properties of Mg-doped $LiTaO_3$ ceramics, *Mater. Res. Bull.*, **39**, [14], 2229 – 2240, (2004).

17 Lin, P.J., Bursill, L.A.: High-resolution study of $Li_{(1-x)}Ag_xTaO_3$, *Micron.*, **13**, [3], 275 – 27, (1982).

18 Chao, S., Dogan, F.: Effects of manganese doping on the dielectric properties of titanium dioxide ceramics, *J. Am. Ceram. Soc.*, **94**, [1], 179 – 186, (2011).

19 Kulawik, J., Szwagierczak, D.: Dielectric properties of manganese and cobalt doped lead iron tantalate ceramics, *J. Eur. Ceram. Soc.*, **27**, [5], 2281 – 2286, (2007).

20 Wang, C.C., Ni, W., Zhang, D., Sun, X., Zhang, N.: Dielectric properties of pure and Mn-doped $CaCu_3Ti_4O_{12}$ ceramics over a wide temperature range, *J. Electroceram.*, **36**, [1 – 4], 46 – 57, (2016).

21 Li, X.J., Wang, Q., Li, Q.L.: Effects of MnO_2 addition on microstructure and electrical properties of $(Bi_{0.5}Na_{0.5})0.94Ba0.06TiO_3$ ceramics, *J. Electroceram.*, **20**, [2], 89 – 94, (2008).

22 Ng, Y.S., Alexander, S.M.: Structural studies of manganese stabilised lead-zirconate-titanate, *Ferroelectrics*, **60**, [1], 79 – 79, (1984).

23 Yan, Y., Kyung-Hoon Cho, Priya, S., Feteira, A.: Identification and effect of secondary phase in MnO_2-doped $0.8Pb(Zr_{0.52}Ti_{0.48})O_3$-$0.2Pb(Zn_{1/3}Nb_{2/3})O_3$ piezoelectric ceramics, *J. Am. Ceram. Soc.*, **94**, [11], 3953 – 3959, (2011).

24 Hou, Y.D., Lu, P.X., Zhu, M.K., Song, X.M., Tang, J.L., Wang, B., Yan, H.: Effect of MnO_2 addition on the structure and electrical properties of $Pb(Zn_{1/3}Nb_{2/3})0.20(Zr_{0.50}Ti_{0.50})0.80O_3$ ceramics, *Mater. Sci. Eng., B*, **116**, [1], 104 – 108, (2005).

25 Cen, Z., Wang, X., Huan, Y., Zhen, Y., Feng, W., Li, L.: Defect engineering on phase structure and temperature stability of KNN-based ceramics sintered in different atmospheres, *J. Am. Ceram. Soc.*, **101**, [7], 3032 – 3043, (2018).

26 La Rosa-Toro, A., Berenguer, R., Quijada, C., Montilla, F., Morallón, E., Vázquez, J.L.: Preparation and characterization of copper-doped cobalt oxide electrodes, *J. Phys. Chem. B.*, **110**, [47], 24021 – 24029, (2006).

27 Wang, L., Wei, R., Ma, W., Ming, L., Peng, S., Wu, X.: Improved electrical properties for Mn-doped lead-free piezoelectric potassium sodium niobate ceramics, *Aip. Adv.*, **5**, [9], 66 – 51, (2015).

28 Huan, Y., Wang, X., Wei, T., Zhao, P., Xie, J., Ye, Z.: Defect control for enhanced piezoelectric properties in SnO_2 and ZrO_2 co-modified KNN ceramics fired under reducing atmosphere, *J. Eur. Ceram. Soc.*, **37**, [5], 2057 – 2065, (2017).

29 Xiao, M., Wei, Y., Zhang, P.: The effect of sintering temperature on the crystal structure and microwave dielectric properties of $CaCoSi_2O_6$ ceramic, *Mater. Chem. Phys.*, **225**, 99 – 104, (2019).

30 Sun, Y., Liu, H., Hao, H., Zhang, S.: Effect of oxygen vacancy on electrical property of acceptor doped $BaTiO_3$-$Na_{0.5}Bi_{0.5}TiO_3$-Nb_2O_5 X8R systems, *J. Am. Ceram. Soc.*, **99**, [9], 3067 – 3073, (2016).

31 Guo, Q., Hou, L., Li, F., Xia, F., Wang, P., Hao, H., Sun, H., Liu, H., Zhang, S: Investigation of dielectric and piezoelectric properties in aliovalent Eu^{3+}-modified $Pb(Mg_{1/3}Nb_{2/3})O_3$-$PbTiO_3$ ceramics, *J. Am. Ceram. Soc.*, [12], 7428 – 7435, (2019).